https://dx.doi.org/10.22161/ijaers.4.12.20 *ISSN: 2349-6495(P) | 2456-1908(O)*

Construction of an Instrumentation Kit for Identification and Control of DC Motors

Lucas Niro[1], Wagner de S. Chaves[2], Eduardo H. Kaneko[3], Matheus F. Mollon[4], Marcio A. F. Montezuma[5]

[1,5]Department of Mechanical Engineering, University of Technology - Paraná, Cornélio Procópio, Paraná, Brazil
[2,3,4] Graduate Student, University of Technology - Paraná, Cornélio Procópio, Paraná, Brazil

Abstract**—** *This paper presents the development of an instrumentation kit of voltage and current measurement for identification of the dynamic model and control of direct current (DC) motors. In the methodology for the parameters identification is used the responses of input voltage and current, and angular velocity of the DC motor. The validation of the obtained dynamic model is done through the comparison of the simulated and experimental responses, and the application of a control system based on state feedback and complete eigenstructure assignment (tracking system). The responses are compared through the normalized root-mean-square error criterion.*

Keywords— Control Systems, Parameters Identification.

I. INTRODUCTION

Direct current (DC) motors are widely used in engineering, e.g. in the position control of a robotic arm. The DC motor guarantees a good torque generation and is efficient for speed control. In some cases, for the design of control systems it is necessary to have an accurate dynamic model of the DC motor [1, 2, 3].

The use of experimental methods allows the determination of the dynamic model of a DC motor. An example of identification methodology is presented in [3]. Where the identification of the dynamic model parameters is done by measuring the motor speed response that results from the application of a constant voltage input.

In this context, this work presents the construction of an instrumentation kit for identification of the dynamic model and control of DC motors. Thus, allowing the study of different identification techniques, and the practical study of control techniques, such as those seen in [4, 5, 6, 7].

The methodology to identify the model of the DC motor recalls [8]. The effectiveness of the identification methodology is demonstrated by the comparison of the dynamic model and the real system responses. This paper also presents the control of a DC motor, using the instrumentation kit, through the tracking control system that uses state feedback and complete eigenstructure assignment. The normalized root-mean-square error (NRMSE) is used to analyze the responses.

The work is organized as follows. Section II presents the linear state space model for a DC motor. In Section III is presented the development of the instrumentation kit. In Section IV, the methodology for the identification is presented. Section V describes the design of the tracking system that uses state feedback and complete eigenstructure assignment. In Section VI is shown the configuration of the experiments and the results obtained. Section VII concludes this paper.

II. DC MOTOR DYNAMIC MODEL

A common linear state space model for the motor is given in (1) and (2), where the angular velocity ω_m and the direct current I_a are the states. The variable J is the moment of inertia of the rotor, b is the viscous friction constant, K_e is the electromotive force constant, K_t is the motor torque constant, R_a is the armature resistance, L_a is the armature inductance and V_a is the supply voltage.

$$\frac{d}{dt}\begin{bmatrix}\omega_m \\ I_a\end{bmatrix} = \begin{bmatrix}-b/J & K_t/J \\ -K_e/L_a & -R_a/L_a\end{bmatrix}\begin{bmatrix}\omega_m \\ I_a\end{bmatrix} + \begin{bmatrix}0 \\ 1/L_a\end{bmatrix}V_a \quad (1)$$

$$y = [1 \quad 0]\begin{bmatrix}\omega_m \\ I_a\end{bmatrix} \quad (2)$$

This state space model may vary depending on the work. In [9] is presented a model with a few differences. The work developed in [10] shows the mathematical model of a DC motor with the angular position as a state.

III. INSTRUMENTATION KIT EVELOPEMENT

The instrumentation kit was built inside the case of a broken function generator, reusing its linear voltage source that was still functional. This approach was important for reducing the cost, and contributed for the recycling of electronic waste.

To identify a DC motor it is necessary to acquire its input voltage and current, in addition to its angular velocity. Based on this, the voltage (LV 25-P) and current (LA 25-NP) sensors were established. An encoder with 100 counts per-revolution was used to measure the angular velocity. The function generator's linear voltage source was reused

https://dx.doi.org/10.22161/ijaers.4.12.20 *ISSN: 2349-6495(P) | 2456-1908(O)*

to power up the sensors, as it generates a voltage of -16 V to 16 V with 1 A of direct current.

Once the sensors were established, it was necessary to define the acquisition ranges. The DC motor used has a nominal voltage of 12 V and peak current of 1 A. Then, the acquisition range for the voltage sensor was defined from -12 V to 12 V and for the current sensor was defined from -5 A to 5 A. Both transducers require an input voltage of -12 V to 12 V to operate correctly, so a voltage regulator lowers the voltage of the power supply from the -16 V to 16 V range to the -12 V to 12 V range.

Since the sensor's output is a very low current, it must be amplified. The INA 121 operational amplifier was used and the output range was normalized from -10 V to 10 V, according to the analog input range of National Instruments NI-PCI 6251 acquisition system.

The schematic of the designed voltage sensor circuit is shown in Fig. 1. It reads the input voltage range of -12 V to 12 V, resulting in a voltage normalized from -10 V to 10 V.

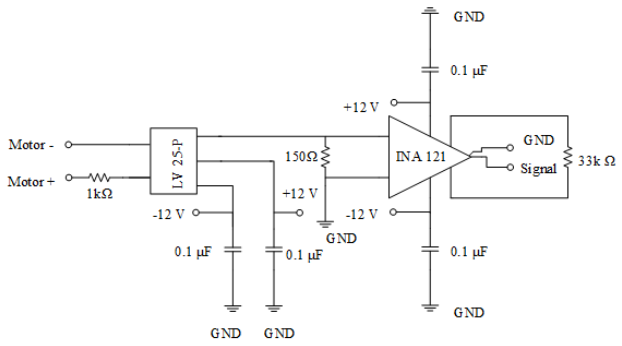

Fig. 1: Voltage sensor circuit schematic.

Through the datasheets of the voltage sensor and the INA 121, it was determined the theoretical equation of the voltage sensor circuit, presented in (3), where V_{in} is the input voltage and V_{out1} is the output voltage from the Fig. 1 circuit. The voltage sensor has a gain of 2.5 times the input current. The output current of the LV 25-P passes through a resistor of 150 Ω. This voltage drop across the resistor is amplified by INA 121, which has a gain of $\left(1 + (50/33)\right)$.

$$V_{out1} = 2.5 * 150 * \left(1 + \left(\frac{50}{33}\right)\right) * \frac{V_{in}}{1000} \ldots\ldots\ldots\ldots (3)$$

The design procedure of the current sensor circuit is analogous to that of the voltage sensor circuit, the only difference is that a resistor is not required at the input. The LA 25-NP has several settings for measured current, for this application, it was configured for up to 5A. The schematic of the current sensor circuit is shown in Fig. 2.

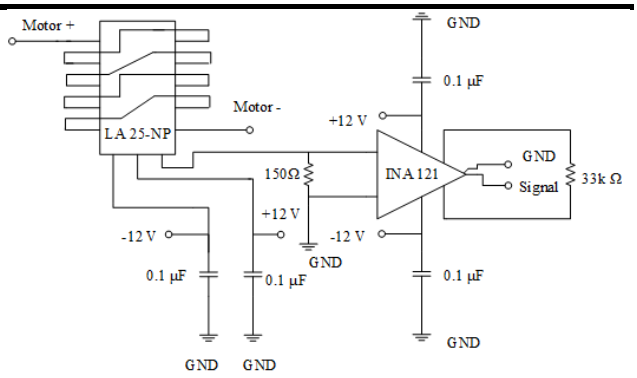

Fig. 2: Current sensor circuit schematic.

It is verified through the schematic that the theoretical equation of the current sensor circuit is practically the same as the voltage sensor circuit. The only difference is that the gain of the sensor is $5/1000$, as shown in (4), where I_{in} is the input current and V_{out2} is the output voltage from the Fig. 2 circuit.

$$V_{out2} = \frac{5}{1000} * 150 * \left(1 + \left(\frac{50}{33}\right)\right) * I_{in} \ldots\ldots\ldots\ldots (4)$$

The theoretical equations of the circuits in (3) and (4) present a first estimate of the values to be obtained. However, some simplifications were made in this process, such as neglecting the sensor induction coil. Therefore, it is necessary to carry out a calibration of the two circuits.

The calibration process consists of applying a known voltage and current, respectively, to the circuits of the voltage and current sensors, and measuring the resulting output voltages. The 0 V to 10 V range is chosen since it is the default range and is supported by the acquisition board. Both sensors have current as input quantity. The voltage sensor circuit requires a fixed 1 kΩ resistor to transform the voltage applied to the motor into current, attending the input range of the sensor. A variable voltage source and a resistor of 0.4 Ω with 10 W were used in the calibration of the current sensor to generate a known input current. Figs. 3 and 4 show the calibration procedure, respectively, for the voltage and current sensors.

Fig. 3: Calibration experiment for the voltage sensor.

https://dx.doi.org/10.22161/ijaers.4.12.20 *ISSN: 2349-6495(P) | 2456-1908(O)*

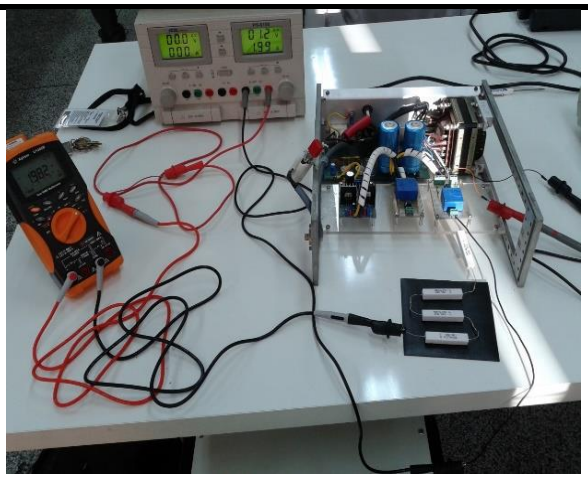

Fig. 4: Calibration experiment for the current sensor.

Figs. 5 and 6 show the data points obtained experimentally and the curves fitted by the least squares method, respectively, for the voltage and current sensors.

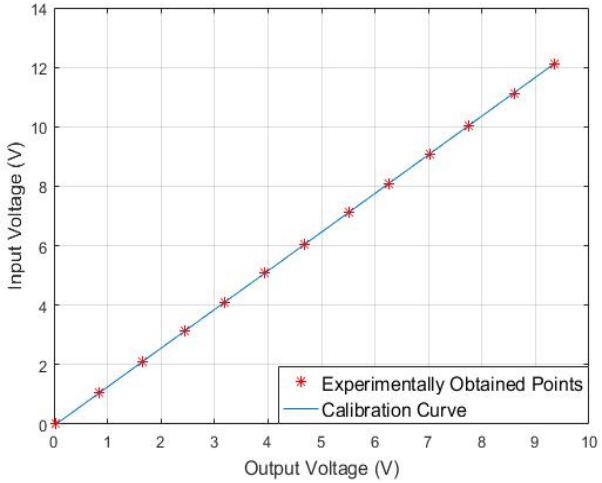

Fig. 5: Calibration curve for the voltage sensor.

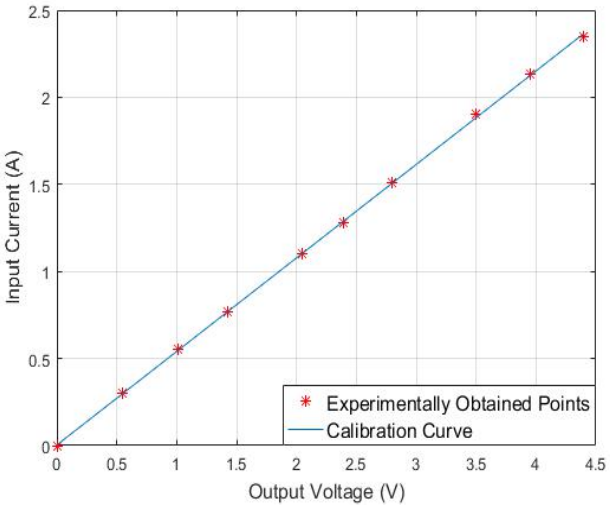

Fig. 6: Calibration curve for the current sensor.

The equations of the fitted curves are presented in (5) and (6) for the voltage and current sensors, respectively. The variable V_{in} is the motor input voltage, V_{out1} is the output from the voltage sensor circuit, I_{in} is the motor input current and V_{out2} is the output from the current sensor circuit.

$$V_{in} = 1.3017\, V_{out1} - 0.0511 \quad \ldots\ldots (5)$$

$$I_{in} = 0.5369\, V_{out2} + 0.0035 \quad \ldots\ldots (6)$$

The inside view of the kit is presented in Fig. 7, where the linear voltage source, voltage regulator, and voltage and current sensor circuits are highlighted. Fig. 8 shows the complete instrumentation kit.

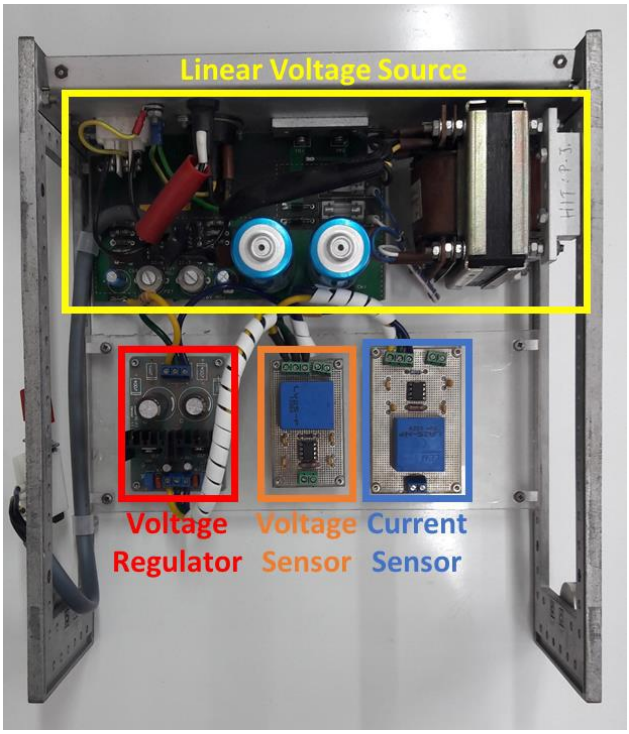

Fig. 7: Inside view of the instrumentation kit.

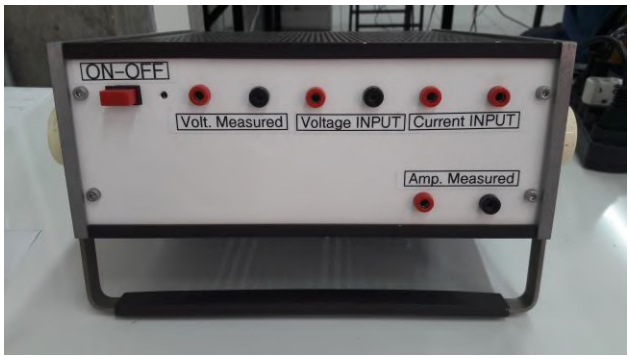

Fig. 8: Instrumentation kit.

IV. IDENTIFICATION METHOD

The identification method starts from the second-order model presented in Fig. 9, formed by two blocks of first-order transfer functions. The first block, from left to right, of first-order is the electric part and the second first-order block is the mechanical part of the motor. The input of the model is the voltage applied to the motor terminals and the output is the angular velocity of the motor.

https://dx.doi.org/10.22161/ijaers.4.12.20 *ISSN: 2349-6495(P) | 2456-1908(O)*

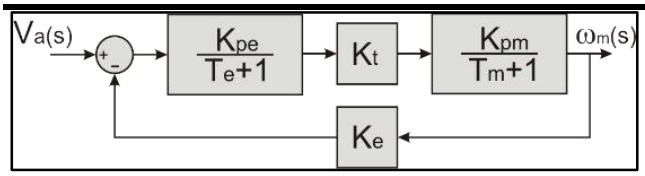

Fig. 9: Block diagram for the DC motor model.

The first step of the identification method is to obtain the armature resistance R_a. This procedure consists of applying a known low voltage V_a directly to the motor terminals, locking the shaft so that it does not rotate, and measuring the motor current I_a. The armature resistance is obtained by (7).

$$R_a = \frac{V_a}{I_a} \quad (7)$$

After obtaining the value of R_a, it is calculated the electromotive force constant K_e. In this experiment a known voltage V_a is applied to the motor, and the angular velocity ω_m and current I_a are measured. The electromotive force constant is found by (8). For this method, the torque constant K_t presented in Fig. 9 has the same value as K_e.

$$K_e = \frac{(V_a - I_a R_a)}{\omega_m} \quad (8)$$

In order to identify the parameters of the electric and mechanical blocks, it is necessary to create the input and output vectors shown in Fig. 10. In this experiment, the motor is subjected to a step input with amplitude equal to its nominal voltage. The angular velocity and current responses are acquired to create the input and output vectors shown in Fig. 10.

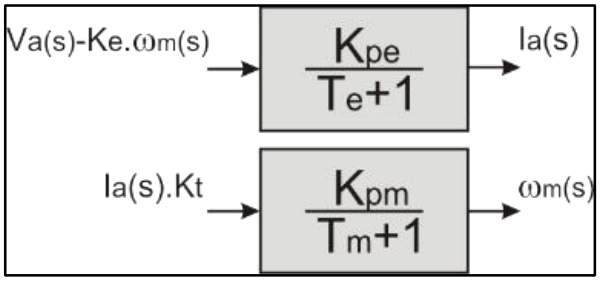

Fig. 10: Input and output vectors for estimation of the first-order blocks.

The parameters of the first-order functions are identified using the functions from the System Identification Tools of the MATLAB/Simulink software. This gives the values of K_{pe}, T_e, K_{pm} and T_m, concluding the identification methodology for the proposed second-order model.

V. TRACKING SYSTEM

The tracking control system is illustrated in Fig. 11.

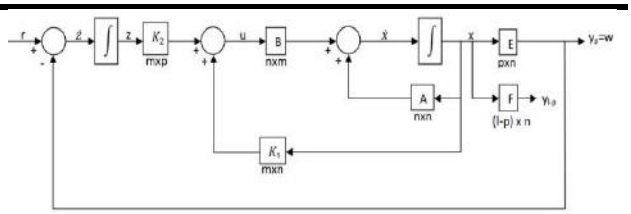

Fig. 11: Tracking control system.

For the tracking system design, a controllable open-loop system is represented by the n th-order state and the p th-order output presented, respectively, in (9) and (10) [11].

$$\dot{\boldsymbol{x}} = \boldsymbol{Ax} + \boldsymbol{Bu} \quad (9)$$

$$\boldsymbol{y} = \boldsymbol{Cx} = \begin{bmatrix} \boldsymbol{E} \\ \boldsymbol{F} \end{bmatrix} \boldsymbol{x} \quad (10)$$

where $\boldsymbol{y}$ is a $p \times 1$ vector and $\boldsymbol{w} = \boldsymbol{Ex}$ is a $m \times 1$ vector that represents the outputs required to follow a $m \times 1$ input vector $\boldsymbol{r}$. As presented in [11] the design method consists of adding a vector comparator and an integrator, satisfying (11).

$$\dot{\boldsymbol{z}} = \boldsymbol{r} - \boldsymbol{w} = \boldsymbol{r} - \boldsymbol{Ex} \quad (11)$$

According to [12] the state feedback control law that is used here is given in (12). This control law assigns, if and only if the matrices pair $(\bar{\boldsymbol{A}}, \bar{\boldsymbol{B}})$ is controllable, the desired closed loop eigenvalues spectrum [11].

$$\boldsymbol{u} = \boldsymbol{K_1 x} + \boldsymbol{K_2 z} = [\boldsymbol{K_1} \quad \boldsymbol{K_2}] \begin{bmatrix} \boldsymbol{x} \\ \boldsymbol{z} \end{bmatrix} \quad (12)$$

The pair $(\bar{\boldsymbol{A}}, \bar{\boldsymbol{B}})$ is controllable if it satisfies (13) and the pair $(\boldsymbol{A}, \boldsymbol{B})$ satisfies the controllability condition in (14) [11].

$$rank \begin{bmatrix} \boldsymbol{B} & \boldsymbol{A} \\ \boldsymbol{0} & -\boldsymbol{E} \end{bmatrix} = n + m \quad (13)$$

$$rank\ \boldsymbol{M_c} = rank[\boldsymbol{B}\ \boldsymbol{AB}\ \boldsymbol{A^2 B} \ldots \boldsymbol{A^{n-m} B}] = n \quad (14)$$

When conditions in (13) and (14) are satisfied, it is guaranteed that the control law given in (15) can be synthesized, in a way that the command input is tracked by the closed-loop output. The closed-loop state equation, for this case, is given in (15) [11].

$$\dot{\boldsymbol{x}}' = \begin{bmatrix} \dot{\boldsymbol{x}} \\ \dot{\boldsymbol{z}} \end{bmatrix} = \begin{bmatrix} \boldsymbol{A} + \boldsymbol{BK_1} & \boldsymbol{BK_2} \\ -\boldsymbol{E} & \boldsymbol{0} \end{bmatrix} \begin{bmatrix} \boldsymbol{x} \\ \boldsymbol{z} \end{bmatrix} + \begin{bmatrix} \boldsymbol{0} \\ \boldsymbol{I} \end{bmatrix} \boldsymbol{r} \quad (15)$$

The gains $\boldsymbol{K_1}$ and $\boldsymbol{K_2}$ of the control system were found by the eigenstructure assignment methodology proposed in [11]. The eigenvalues are selected to assign performance characteristics over time. For the closed-loop plant matrix in (15), the eigenvalues must be in the left-half plane of the complex plane and belong to the null vector space $\aleph$ (i.e. vectors that represent the solutions to the matrix $[\boldsymbol{A} - \boldsymbol{\lambda_i I} \quad \boldsymbol{B}]$), this is done by the selection of the feedback matrix [11].

In this way, the piecewise constant command vector $\boldsymbol{r}(t)$ is tracked by the outputs $\boldsymbol{w}(t)$, in the steady state. The $\ker S(\lambda_i)$ imposes constraints on the eigenvector $\boldsymbol{v_i}$, this may be associated with the assigned eigenvalue λ_i. A specific subspace is identified by the $\ker S(\lambda_i)$, and the

https://dx.doi.org/10.22161/ijaers.4.12.20 *ISSN: 2349-6495(P) | 2456-1908(O)*

chosen eigenvectors $\boldsymbol{v_i}$ must be located within this subspace [11].

VI. EXPERIMENTS AND RESULTS

The workbench where the experiments were performed consists of a computer with Windows XP operating system with the MATLAB/Simulink software running in Real-Time Windows Target mode. The National Instruments NI-PCI 6251 card is installed on this computer to perform the reading of the encoders, the acquisition of the voltage and current signals from the instrumentation kit sensors and the control of the motor, through a linear power drive. The DC motor identified and controlled is the Maxon F2140 motor, and is powered by the Maxon LSC 30-2 linear power drive. The complete experiment workbench is shown in Fig. 12.

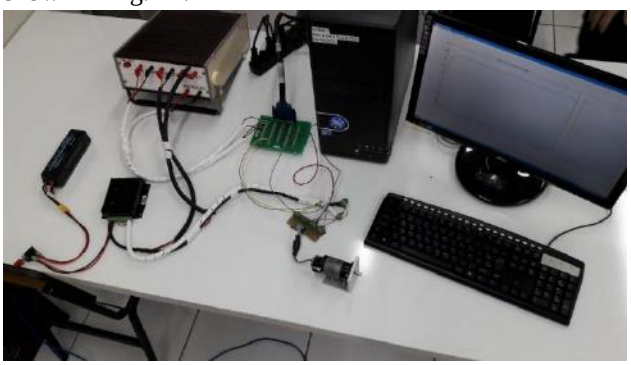

Fig. 12: Experimental workbench for identification and control.

The transfer functions resulting from the identification of the Maxon F2140 motor are presented in (16) and (17), respectively, for the models of current and angular velocity.

$$\frac{Ia}{Va} = \frac{0{,}06309s + 0{,}09498}{0{,}001339s^2 + 0662s + 20{,}44} \quad \ldots\ldots\ldots\ldots\ldots (16)$$

$$\frac{\omega m}{Va} = \frac{699{,}4}{0{,}001339s^2 + 0662s + 20{,}44} \quad \ldots\ldots\ldots\ldots\ldots (17)$$

The comparison between the experimental and simulated results are shown in Figs. 13 and 14, respectively, for current and angular velocity. Tables 1 and 2 shows the comparison between the experimental and simulated results using the NRMSE.

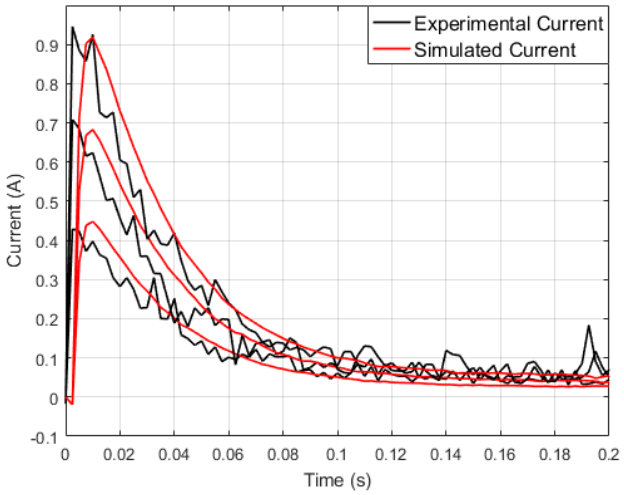

Fig. 13: Experimental and simulated current.

Table 1: Comparison between experimental and simulated current responses.

Voltage (V)	NRMSE (%)
11.5	72.38
8.5	63.40
5.6	48.53

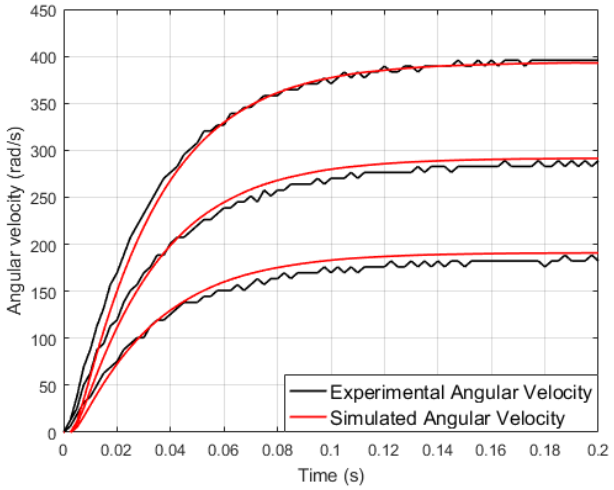

Fig. 14: Experimental and simulated angular velocity.

Table 2: Comparison between experimental and simulated angular velocity responses.

Voltage (V)	NRMSE (%)
11.5	84.45
8.5	86.00
5.6	68.77

It is verified that the model identified for the nominal motor voltage (11.5 V), which represents the current peak of 0.9 A and the angular velocity of 400 rad/s, is the closest to the real behavior of the DC motor. In order to validate the identified model, it was subjected to a voltage of 8.5 V

https://dx.doi.org/10.22161/ijaers.4.12.20 *ISSN: 2349-6495(P) | 2456-1908(O)*

and 5.6 V, as it is possible to analyze from Figs. 13 and 14, and Tables 1 and 2.

In Figs. 15 and 16 are presented the responses for the tracking control system with a square wave input, respectively, for the angular velocity and control action. Table 3 presents the NRMSE to analyze the accuracy of the control responses for the square wave input.

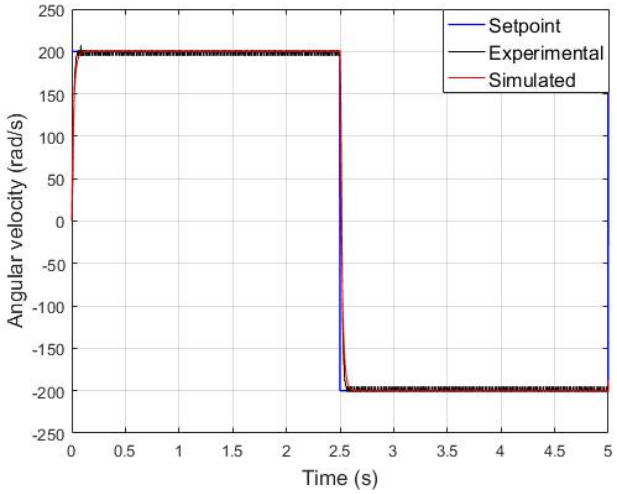

Fig. 15: Angular velocity response for the square wave input.

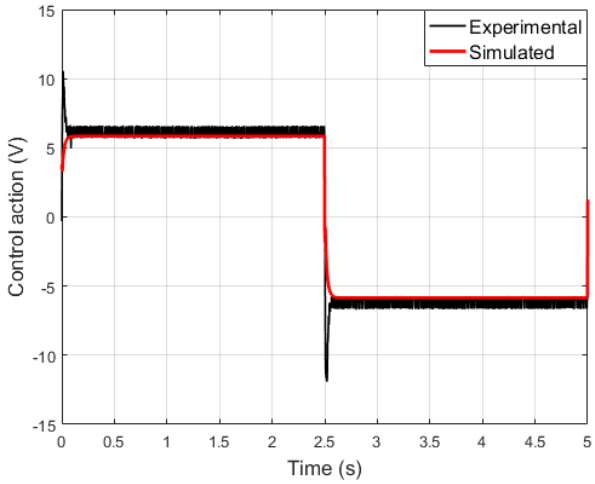

Fig. 16: Control action response for the square wave input.

Table 3: Comparison between experimental and simulated control responses for square wave input.

Response	NRMSE (%)
Angular Velocity (rad/s)	97.27
Control Action (V)	85.68

Figs. 17 and 18 present the responses for the tracking control system with a sine wave input, respectively, for the angular velocity and control action. Table 4 presents the NRMSE to analyze the accuracy of the control responses for the sine wave input.

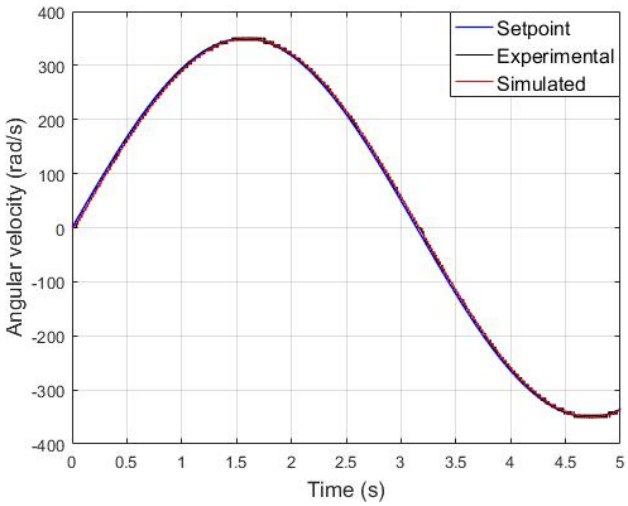

Fig. 17: Angular velocity response for the sine wave input.

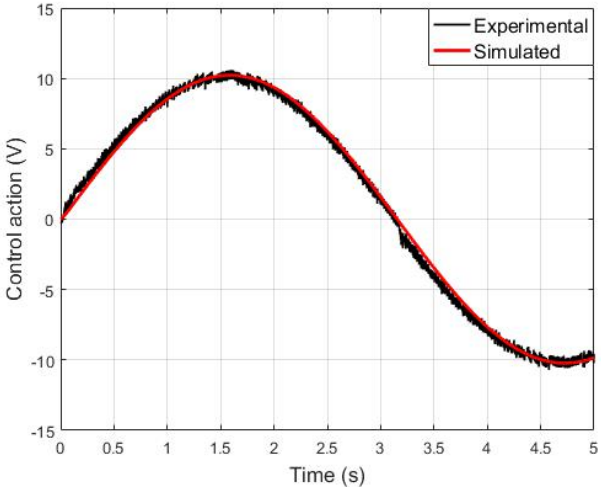

Fig. 18: Control action response for the sine wave input.

Table 4: Comparison between experimental and simulated control responses for sine wave input.

Response	NRMSE (%)
Angular Velocity (rad/s)	98.82
Control Action (V)	93.87

VII. CONCLUSIONS

This article presented the development of an instrumentation kit, which composes an experimental workbench, with the purpose of identifying the dynamic model and controlling DC motors. In general, all purposes of the developed instrumentation kit have been met.

The methodology used in the identification of the dynamic model presented satisfactory results for the Maxon F2140 motor. As the dynamic model of this motor was identified from the input voltage and current responses resulting from the application of a step signal with the amplitude voltage of 11.5V, it was expected that the simulated response from the model and the experimental response from the actual

https://dx.doi.org/10.22161/ijaers.4.12.20 *ISSN: 2349-6495(P) | 2456-1908(O)*

system would be close. This was proved by the calculated NRMSE criterion presented in Tables 1 and 2.

As the dynamic model was tested for input signals with amplitudes smaller than the nominal voltage, it was possible to observe that the proximity between the experimental and simulated responses decreases, as seen in Figs. 13 and 14 and proved by the calculated NRMSE presented in Tables 1 and 2. However, the loss of accuracy in this extrapolation is considered satisfactory when considering the actual behavior of a DC motor. This satisfactory variation in extrapolation is due to the planning of the instrumentation kit and especially the choice to use a linear power drive.

The tracking control system with state feedback and complete eigenstructure assignment proved to be efficient for DC motor control, as evidenced by the responses and the NRMSE criterion for square and sine wave inputs. As seen from Tables 3 and 4 the square wave response was less accurate than the sine wave response. This was expected considering the sudden changes in the setpoint represented by a square wave.

As advantages of the instrumentation kit, it is possible to present the easiness for installing in the experimental workbench and connecting with the acquisition system. In addition, the whole structure of the experimental workbench was interesting because it allowed the execution of identification and control in a single software, being it MATLAB/Simulink or LabVIEW. The reuse of electronic waste is also an interesting feature of the work developed.

The main limitations of the instrumentation kit are related to the voltage and current acquisition ranges. The voltage sensor circuit is designed to measure a maximum of 12V, the change of this limit can be made by altering the input resistor and performing a new calibration. The current sensor circuit was designed to measure a maximum of 5A, changing this limit depends on changing the circuit design for a different configuration of the LA 25-NP sensor.

REFERENCES

[1] H. Karimipour and H. Toosian shandiz, “A new adaptive fuzzy controller for DC motor position control,” 2009 Fifth International Conference on Soft Computing, Computing with Words and Perceptions in System Analysis, Decision and Control, Famagusta, 2009, pp. 1-4.

[2] N. Saikumar and N. S. Dinesh, “Improved adaptation of EMPC with response sampling based prediction correction for the position control of DC motors,” 2014 International Conference on Computer, Control, Informatics and Its Applications (IC3INA), Bandung, 2014, pp. 109-114.

[3] W. Wu, “DC motor identification using speed step responses,” Proceedings of the 2010 American Control Conference, Baltimore, MD, 2010, pp. 1937-1941.

[4] M. A. Darwish and H. S. Abbas, “DC motor position control using discrete-time fixed-order H∞ controllers,” 2012 First International Conference on Innovative Engineering Systems, Alexandria, 2012, pp. 260-265.

[5] G. h. Chang, Y. f. Li and Q. Gang, “Intelligent controller design for PM DC motor position control using evolutionary programming,” 2011 IEEE 2nd International Conference on Computing, Control and Industrial Engineering, Wuhan, 2011, pp. 37-40.

[6] A. Lichtman and P. Fuchs, “Theory of PI controller and introduction to implementation for DC motor controls,” 2017 Communication and Information Technologies (KIT), Vysoke Tatry, 2017, pp. 1-5.

[7] N. Daksha and K. Rudraksha, “Design and testing of self-tuned fuzzy PI controller for improved speed control and accelerating torque characteristics of a DC motor,” 2017 4th International Conference on Power, Control & Embedded Systems (ICPCES), Allahabad, India, 2017, pp. 1-6.

[8] V. A. Oliveira, M. L. Aguiar and J. B. Vargas. Sistemas de controle: aulas de laboratório. 2nd ed. EESC-USP, 2013.

[9] P. Deshpande and A. Deshpande, “Inferential control of DC motor using Kalman Filter,” 2012 2nd International Conference on Power, Control and Embedded Systems, Allahabad, 2012, pp. 1-5.

[10] M. A. Aravind, N. Saikumar and N. S. Dinesh, “Optimal position control of a DC motor using LQG with EKF,” 2017 International Conference on Mechanical, System and Control Engineering (ICMSC), St. Petersburg, 2017, pp. 149-154.

[11] J. D’azzo and C. Houpis. Linear control system analysis and design: conventional and modern. 4th ed. New York: McGraw-Hill Companies, 1995.

[12] M. A. F. Montezuma. Methodology for identification and control of a movement platform prototype with 2 D.O.F. Ph.D. Dissertation, School of Engineering of São Carlos, University of São Paulo, São Carlos, 2010.